Vinculin acts as a sensor in lipid regulation of adhesion-site turnover

Indra Chandrasekar[1], Theresia E. B. Stradal[2], Mark R. Holt[3], Frank Entschladen[4], Brigitte M. Jockusch[1] and Wolfgang H. Ziegler[1,*,‡]

[1]Cell Biology, Zoological Institute, Technical University of Braunschweig, 38106 Braunschweig, Germany
[2]Cell Biology, German Research Centre for Biotechnology (GBF), 38124 Braunschweig, Germany
[3]The Randall Division, King's College London, London SE1 1UL, UK
[4]Institute of Immunology, Witten/Herdecke University, 58448, Witten, Germany
*Present address: IZKF-Interdisciplinary Centre for Clinical Research Leipzig, Faculty of Medicine, University of Leipzig, 04103 Leipzig, Germany
‡Author for correspondence (e-mail: wolfgang.ziegler@medizin.uni-leipzig.de)

Accepted 18 January 2005
Journal of Cell Science 118, 1461-1472 Published by The Company of Biologists 2005
doi:10.1242/jcs.01734

Summary

The dynamics of cell adhesion sites control cell morphology and motility. Adhesion-site turnover is thought to depend on the local availability of the acidic phospholipid phosphatidylinositol-4,5-bisphosphate (PIP_2). PIP_2 can bind to many cell adhesion proteins such as vinculin and talin, but the consequences of this interaction are poorly understood. To study the significance of phospholipid binding to vinculin for adhesion-site turnover and cell motility, we constructed a mutant, vinculin-LD, deficient in acidic phospholipid binding yet with functional actin-binding sites. When expressed in cells, vinculin-LD was readily recruited to adhesion sites, as judged by fluorescence recovery after photobleaching (FRAP) analysis, but cell spreading and migration were strongly impaired, and PIP_2-dependent disassembly of adhesions was suppressed. Thus, PIP_2 binding is not essential for vinculin activation and recruitment, as previously suggested. Instead, we propose that PIP_2 levels can regulate the uncoupling of adhesion sites from the actin cytoskeleton, with vinculin functioning as a sensor.

Supplementary material available online at
http://jcs.biologists.org/cgi/content/full/118/7/1461/DC1

Key words: Cell-matrix adhesion, Cell motility, Microfilaments, Phosphatidylinositol-4,5-bisphosphate, Vinculin

Introduction

Cell migration requires a regulated interplay of actin-filament dynamics and turnover of cell-matrix adhesions (Pollard and Borisy, 2003; Ridley et al., 2003). Both processes are mechanically coupled by a large complex of cytoplasmic proteins linking integrins (the transmembrane receptors) to the actin cytoskeleton (Critchley, 2000; Zamir et al., 1999). Recent progress in the understanding of integrin function indicates a central role for talin in adhesion-site regulation (Giannone et al., 2003; Tadokoro et al., 2003). Binding of talin to integrin β chains induces activation of integrins, leading to high-affinity binding of extracellular matrix proteins (Calderwood et al., 2002; Garcia-Alvarez et al., 2003; Tadokoro et al., 2003) and concomitant force coupling of nascent cell-matrix adhesions to the actin cytoskeleton (Giannone et al., 2003; Jiang et al., 2003). This process activates talin, exposes binding sites for vinculin (Papagrigoriou et al., 2004) and induces the recruitment of vinculin to adhesion sites (Galbraith et al., 2002). Simultaneous binding of vinculin to both talin and actin filaments contributes to the mechanical stability of adhesions and affects their regulation. Modulation of vinculin expression has led to the concept that high vinculin levels inhibit cellular motility, whereas low levels promote it (Rodriguez Fernandez et al., 1992; Rodriguez Fernandez et al., 1993). Furthermore, cells deficient in vinculin have difficulties in stabilizing their adhesion, as required for efficient cell spreading, and they migrate much faster than control cells (Xu et al., 1998a; Xu et al., 1998b).

Vinculin activation requires release of an intramolecular head-to-tail interaction. This intramolecular bond blocks the association of the free, not the membrane-associated, form of vinculin with most of its protein ligands (Critchley, 2000). The recently solved structure of vinculin suggests that binding sites for vinculin ligands are structurally distinct but conformationally linked, and activation of vinculin ligand binding requires the simultaneous binding of several ligands (Bakolitsa et al., 2004; Borgon et al., 2004). In vitro, the intramolecular bond can be released by charging either the vinculin head (Vh) with appropriate talin peptides (Bass et al., 2002; Izard et al., 2004) or the vinculin tail (Vt) with acidic phospholipids such as phosphatidylinositol-4,5-bisphosphate (PIP_2) (Hüttelmaier et al., 1998; Weekes et al., 1996). Binding of PIP_2 to vinculin was suggested to promote adhesion-site targeting of vinculin (Gilmore and Burridge, 1996), and biochemical evidence argues strongly for a competition between acidic-phospholipid and actin-filament binding to the vinculin tail (Steimle et al., 1999).

PIP_2 acts as a central regulator of actin dynamics and adhesion-site turnover (Nayal et al., 2004; Yin and Janmey, 2003), and many cytoskeletal proteins involved in cell adhesion

bind to PIP_2 (Sechi and Wehland, 2000). Both activation and integrin binding of talin are dependent on the local availability of PIP_2 (Martel et al., 2001). Elevated local concentrations of PIP_2 can be a consequence of either release from proteins sequestering acidic phospholipids or generation by lipid kinases (Caroni, 2001; Doughman et al., 2003). Type Iγ 661 phosphatidylinositol-4-phosphate 5-kinase (PIP 5-kinase), a lipid kinase that can raise local PIP_2 levels by phosphorylating the ubiquitous precursor molecule phosphatidylinositol 4-phosphate, is recruited to talin in nascent adhesions and triggers adhesion site growth (DiPaolo et al., 2002; Ling et al., 2002). Conversely, strong overexpression of the same kinase leads to breakdown of adhesion sites as a consequence of imbalanced local PIP_2 levels (Ling et al., 2002).

To elucidate the significance of acidic phospholipid binding to vinculin for its intracellular localization, its influence on adhesion-site dynamics and cell motility, we have mutated one or both lipid-binding sites in vinculin while leaving its actin-binding ability largely intact. Expression of full-length vinculin variants in B16-F1 mouse melanoma cells revealed that the targeting and velocity of incorporation of these mutants into adhesion sites were not affected. By contrast, adhesion-site turnover was grossly slowed down in cells expressing a vinculin mutant defective in both lipid-binding sites, associated with a delay in cell spreading and locomotion. These dominant negative effects of this mutant were seen on several different extracellular matrices. Furthermore, disassembly of adhesion sites and detachment of cells, seen as a consequence of increased cellular PIP_2 levels in cells overexpressing PIP 5-kinase, were suppressed. Our results emphasize that vinculin targeting to and incorporation into adhesion sites is independent of lipid binding, whereas adhesion site turnover strongly depends on the vinculin-PIP_2 interaction.

Materials and Methods

Cloning and mutagenesis of vinculin and PIP 5-kinase α expression constructs, and graphical representation

The mouse vinculin-encoding cDNA was obtained by PCR amplification from a mouse heart cDNA library in pACT (BD Biosciences), sequenced and fused into pEGFP-C2 (BD Biosciences). Vinculin head [Vh(1-258)] and tail [Vt(858-1066)] were obtained by PCR amplification, and then sequenced and cloned into pGEX-4T (Amersham Biosciences) or fused to a FLAG tag and cloned into pQE-30 (Qiagen), respectively. The QuikChange® site-directed mutagenesis kit (Stratagene) was used to generate vinculin tail mutants. All mutants were sequenced and subcloned in pQE-30 (Vt) and pEGFP-C2 (full-length). Mouse PIP 5-kinase α in pRK5-Myc (Rozelle et al., 2000) was used to generate a kinase-deficient truncation mutant (Shibasaki et al., 1997) by PCR amplification. The mutant was sequenced, fused to a BiPro tag (Rüdiger et al., 1997) and subcloned into pcDNA3 (Invitrogen). All primers (MWG Biotech) used for PCR cloning and mutagenesis are given in supplementary material. Graphical views of Vt(879-1061) based on PDB entry 1QRK were generated using SwissPDB viewer (http://www.expasy.ch/spdbv/) and POVray 3.1 (http://www.povray.org/) on a Linux platform.

Protein expression, purification and characterization

Recombinant Vt(858-1066) variants were expressed and purified as described (Ziegler et al., 2002). Circular dichroism spectroscopy (J-810 Spectropolarimeter; Jasco) confirmed the α-helical character of Vt variants (Miller et al., 2001). Vh(1-258) bearing an N-terminal glutathione-*S*-transferase (GST) tag was expressed in *Escherichia coli* strain M15, purified on glutathione-Sepharose beads according to manufacturer's instructions (Amersham Biosciences) and used bound to beads in pull-down experiments. Protein concentrations were determined using a BCA assay (Sigma) and identical molar amounts of Vt protein were used in all experiments. However, the Coomassie dye take of Vt proteins was not identical (e.g. 70% and 40% of wild-type (wt) Vt for Vt-H3 and Vt-LD, respectively) and resulted in relatively faint bands of these proteins on Coomassie-stained gels. A comparable effect on the dye take was observed for similar lipid-binding-site mutants of ezrin (Barret et al., 2000).

Vesicle pull-down assay and statistic analysis

Sucrose-loaded large unilamellar vesicles (SLVs) were generated using a mini-extruder (Avanti Polar Lipids) according to manufacturer's instructions, mixed with Vt protein and sedimented. In brief, vesicles containing the phospholipids phosphatidylcholine (PC), phosphatidylserine (PS) (45%) (Sigma) and PIP_2 (7%) (Merck Biosciences) from bovine brain, in molar ratios 4.8:4.5:0.7, were prepared by solubilizing dried phospholipid films in buffer 1 (600 mM sucrose, 100 mM NaCl, 40 mM Tris-HCl pH 7.5 and 3 mM $MgCl_2$). Vesicles were subjected to repeated freeze-thaw cycles (five times) and thereafter to extrusion (11 times) using 0.2 μm filters in a mini-extruder. Vesicles suspension was diluted 1:5 in buffer 2 (100 mM NaCl, 40 mM Tris-HCl pH 7.5, 3 mM $MgCl_2$) and vesicles were collected by high-speed centrifugation, 100,000 ***g*** for 30 minutes in an Airfuge (Beckman Instruments). Vesicles were washed again and finally suspended in buffer 2 (1 mg ml^{-1} total lipid). Proteins were diluted in buffer 2 (5 μM protein, final concentration), precentrifuged at 20,000 ***g*** for 15 minutes to remove any protein aggregates and incubated with SLVs (0.5 mg ml^{-1} final concentration) at 37°C for 15 minutes. After incubation, protein-vesicle mixtures were centrifuged at 20,000 ***g*** for 15 minutes. Pellet and supernatant fractions were separated and proteins retrieved from supernatants by methanol-chloroform precipitation (Wessel and Flügge, 1984). Pellet and supernatant were subjected to SDS-PAGE and Coomassie-stained bands analysed by densitometry (EASY RH apparatus and EASY Image Plus Software; Herolab). Statistical significance of differences in all data sets (unless stated otherwise) was tested by variance analysis (post hoc Bonferroni/Dunn) using Statview 5.0® (SAS Institute). Images were compiled in Adobe® Photoshop® (v.6).

Vinculin tail interaction with Vh (D1) and actin filaments

The interaction of Vt variants with the Vh domain 1 (D1, amino acids 1-258) fragment was tested in a GST pull-down assay. GST-Vh (D1) protein bound to glutathione-Sepharose beads was equilibrated in phosphate buffer (50 mM NaH_2PO_4, pH 7.4, 0.2 mM EGTA) and incubated with Vt proteins (6 μM) for 30 minutes at 37°C. Beads were then washed three times with phosphate buffer. Pellet fractions were analysed on Coomassie-stained SDS-PAGE gels. The interaction of Vt variants with actin filaments was tested by high-speed cosedimentation at various molar ratios of actin and Vt, as described (Ziegler et al., 2002). Prepolymerized actin was used at a 3 μM final concentration. Pellets and supernatants were analysed by densitometry of Coomassie-stained gels (see above). Images were compiled in Adobe Photoshop (v.6).

Cell lines and stable transfection

B16-F1 mouse melanoma cells (ATCC CRL-6323) were cultured in Dulbecco's modified Eagle's medium (DMEM) plus 4.5 g l^{-1} glucose (Invitrogen), 10% foetal calf serum (FCS) (PAA Laboratories), 2 mM glutamine at 37°C and 7% CO_2. Superfect® (Qiagen) was used according to the manufacturer's recommendation for transient and stable transfections. Cells expressing vinculin variants tagged with

green fluorescent protein (GFP) were sorted using a cell sorter (MoFlo; Dako Cytomation) and cultured in the presence of 1 mg ml^{-1} G418 (Invitrogen) to generate stably expressing populations. Following the second round of sorting, cell populations kept under selection pressure were used up to passage six for experiments. Protein expression levels were determined by semiquantitative immunoblotting using a monoclonal vinculin antibody (hVin; Sigma) and densitometry (see above). Blots were scanned and images were compiled in Adobe Photoshop (v.6). For experiments with murine myc-tagged PIP 5-kinase α (Rozelle et al., 2000), wild-type B16-F1 cells or cells stably expressing GFP-vinculin-wt or GFP-vinculin-LD were transfected on coverslips using Superfect (Qiagen) 16 hours after attachment to fibronectin and processed for immunofluorescence as specified below.

Immunofluorescence and video microscopy

After 6 hours of attachment to laminin, cells were fixed with 4% paraformaldehyde (PFA) solution in PBS for 15 minutes, permeabilized with a mixture of 0.1% Triton X-100 in PFA for 60 seconds and blocked with 1% bovine serum albumin (BSA) in PBS. Cell adhesions and actin filaments were stained with mouse anti-paxillin (BD Biosciences) and tetramethylrhodamine isothiocyanate (TRITC) tagged anti-mouse IgG (Sigma) antibodies, and with Alexa-350-coupled phalloidin (Molecular Probes), respectively. In PIP-5-kinase experiments with wild-type B16-F1 cells, actin filaments were stained with Alexa-594-coupled phalloidin and endogenous vinculin using mouse anti-vinculin antibody (Sigma) and Alexa-488-labelled anti-mouse IgG (Molecular Probes). To detect PIP-5-kinase expression, anti-myc antibody 9E10 (Abcam) was used that had been directly coupled to Alexa 350 (Molecular Probes) according to manufacturer's instructions. B16-F1 cells co-expressing PIP5-kinase [or myc-tagged L61-Rac (Lamarche et al., 1996)] with GFP-tagged vinculin variants were stained using a mixture of Alexa-594/phalloidin, and Alexa-350-tagged anti-myc antibody or anti-BiPro 4A6 antibody (Rüdiger et al., 1997) and Alexa-350-labelled anti-mouse IgG (Molecular Probes). Coverslips were mounted using Mowiol® (Aventis). Specimens were examined in a Zeiss Axiovert S100TV microscope using a 100× Plan-Neofluar oil objective (NA 1.3) or a 63× Plan-Neofluar oil objective (NA 1.25) and photographed with a TE/CCD-1000 TKB camera (Princeton Scientific Instruments). To determine the ratio of polarized cells in B16F1 populations, phalloidin-stained cells displaying a clear lamellipodium and trailing edge were scored as motile, cells with several lamellipodia or no clear orientation as ambiguous and cells without lamellipodia as unpolarized. Phalloidin staining was used to improve the visualization of lamellipodia and the orientation of cells. Numbers of polarized, unpolarized and ambiguous cells were counted manually in representative fields (n>600 cells per vinculin variant). Video microscopy was performed as described earlier (Rottner et al., 1999a). All acquisitions and movies were controlled using IPLab software (Scanalytics). Movies were processed by Scion Image software (v.1.6) (Scion). Figures were assembled for presentation using Adobe Photoshop (v.6) and Adobe Illustrator® (v.9).

Adhesion and spreading of cells and migration in collagen matrix

12-well plates (Nunc) were coated with either laminin (25 μg ml^{-1}) or fibronectin (50 μg ml^{-1}) (Sigma) and incubated at room temperature for 1 hour. Alternatively, they were coated with collagen I (1 mg ml^{-1}; Cohesion Technologies) and allowed to polymerize for 3 hours. B16-F1 cells expressing GFP-vinculin variants were harvested in trypsin-EDTA. 1.5×10^4 cells were seeded in each well. For analysis of adhesion, cells were allowed to attach for 10 minutes at 37°C for laminin and fibronectin or 90 minutes for collagen. Nonadherent cells were removed by washing the wells three times with PBS. Cells were fixed in 4% PFA in PBS. The number of cells in ten random microscopic fields (450-550 cells) was counted using a Nikon Eclipse TE 300 with a 10× Plan-Fluar objective (NA 0.3). For analysis of spreading, cells were treated as described above and allowed to attach for 15 minutes at 37°C on laminin or fibronectin. After washing and fixation, cells were stained with TRITC-phalloidin (Sigma) and mounted on slides. Cells were examined in a Zeiss Axiophot microscope using a 40× Plan Neo-Fluar oil objective (NA 1.3) and photographed with a RTE/CCD-1300 Y/HS camera (Roper Scientific). Three subpopulations of cells were counted: spread cells with clear peripheral lamellipodia, non-spread cells (which were just attached) and ambiguous cells that fell in neither of the two categories.

The migratory capacities of the B16-F1 populations expressing GFP-vinculin variants were analysed by time-lapse video microscopy as described (Niggemann et al., 1997). In brief, cells were harvested in trypsin-EDTA and 6×10^4 cells in 50 μl medium were mixed with 100 μl of a carbonate-buffered collagen solution (1.67 mg ml^{-1} bovine dermal type-I collagen). The suspension was filled into self-constructed chambers and the collagen was allowed to polymerize at 37°C for 30 minutes. Migration of the cells was recorded for 15 hours in a 1920-fold time-lapse mode. The paths of 30 randomly selected cells were calculated at 15 minute intervals by computer-assisted cell tracking using custom-made software (Niggemann et al., 1997), and migratory parameters (number of motile cells, velocity, persistence) were calculated from these data.

Analysis of individual adhesion sites (confocal microscopy and FRAP)

Microscopy

B16-F1 cells were microinjected (InjectMan NI 2; Eppendorf) with constructs encoding GFP-vinculin-wt or the -LD mutant. Constructs were allowed to express for 3 hours before mounting coverslips into a chamber containing gassed growth medium. The chamber was placed onto a temperature-regulated 37°C microscope stage 15 minutes before viewing. Time-separated confocal 12-bit images were collected using a Zeiss LSM 510 META confocal laser scanning microscope system with a 63× Plan-Apochromat oil objective (NA 1.4). GFP was excited with the 488 nm line of the argon laser, and reflected and emitted light were separated using a 470-500 nm band-pass filter (for interference reflection microscopy) and a 505 nm long-pass filter (for viewing GFP emission). Line scans were performed with fourfold averaging per pixel. When bleaching, the 488 nm laser line output was set to 100% using 50 iterations. Two images (lines) were scanned before bleaching to determine the pre-bleach intensity of GFP-vinculin. After bleaching, line scans were collected for 3 minutes and stacked together to form a two-dimensional image, a so-called kymograph, in which the x-axis is distance along the line scan and the y-axis represents time with t=0 at the top.

Image analysis

To determine speed of focal-adhesion translocation, adhesions in time-lapse sequences were manually tracked using the Motion Analysis package (Kinetic Imaging). The software calculated the speeds after appropriate calibration. Fluorescence recovery in time-lapse fluorescence recovery after photobleaching (FRAP) sequences was analysed using the Lucida Image Analysis package (Kinetic Imaging). Because focal adhesions had a tendency to translocate, it was not possible to perform a simple spot analysis. Instead, kymographs were produced along the axis of the adhesion sites and the direction of translocation. Five line scans were then taken along the kymograph time axis taking into account any translocation. The average of this was normalized with respect to the initial fluorescence intensity. Normalized values were subtracted using the first post-bleach intensity, which also resulted in background subtraction. The data were then inversely plotted to produce a straight-line graph with

positive gradient. The *x*-axis intercept was used to determine the time constant for fluorescence recovery (i.e. the time taken to recover to a level of 50%). Statistics of data in this paragraph were performed applying an unpaired two-tailed Student's *t*-test (with Welch correction) using InStat3® (GraphPad Software).

Results

Design and characterization of vinculin mutants defective in acidic phospholipid binding

The two lipid-binding sites of vinculin characterized so far consist of clusters of arginine (R) and lysine (K), which form a 'basic ladder' and a 'basic collar' as delineated from the crystal structure of Vt (Bakolitsa et al., 1999) (Fig. 1A). To suppress acidic phospholipid binding to vinculin, we removed positively charged residues from lipid-binding sites by point mutation using a strategy that had been successfully applied earlier to the cytoskeletal proteins α-actinin (Fraley et al., 2003) and ezrin (Barret et al., 2000). As illustrated in Fig. 1B, we mutated to glutamine (Q) four positively charged residues (K952, K956, R963 and K966) in the basic ladder on helix 3 (Vt-H3 mutant), which are not involved in the interactions of

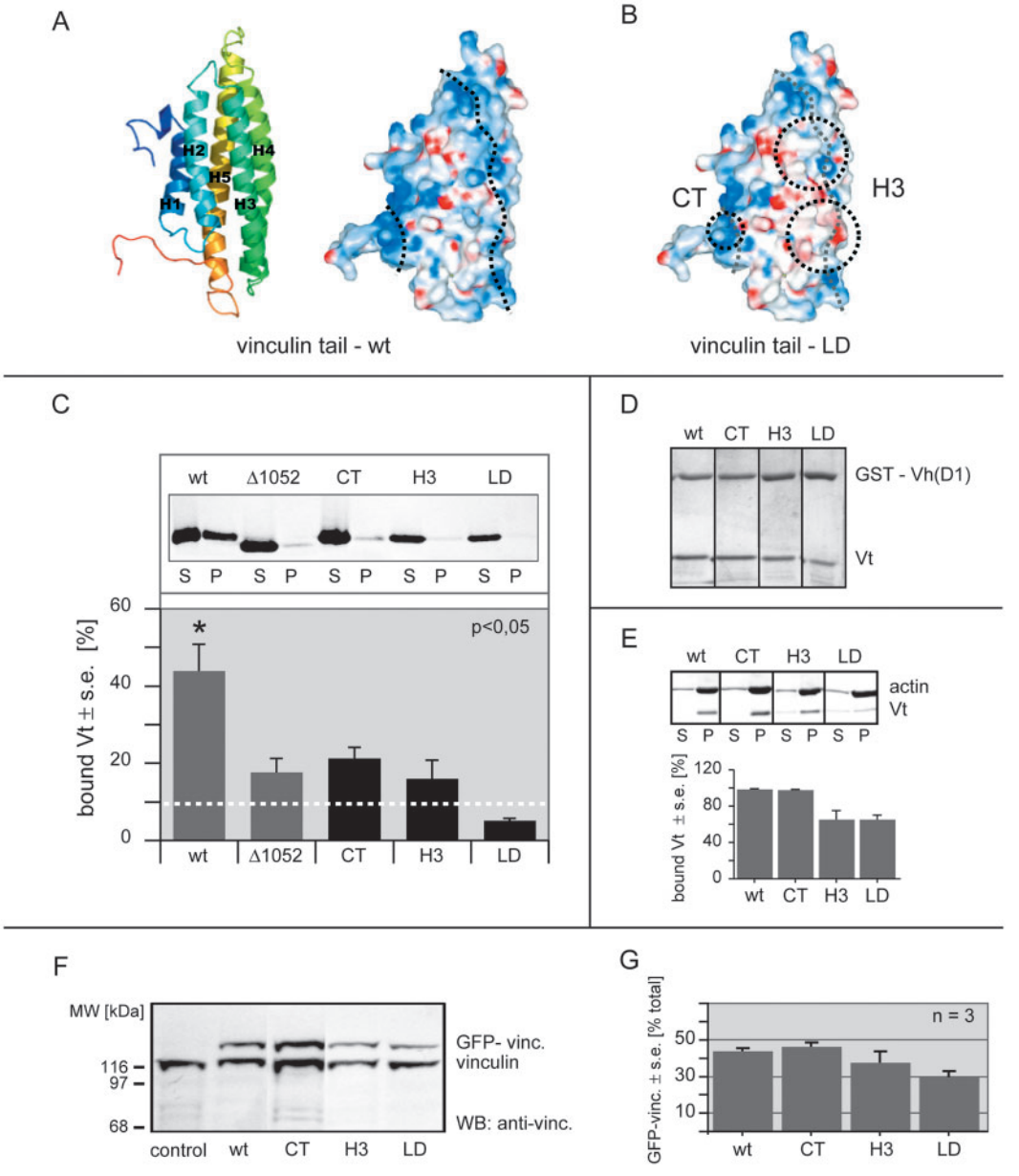

Fig. 1. Mutagenesis of lipid binding sites in vinculin. (A,B) Ribbon and space-filling representations of the vinculin tail (Vt, amino acids 885-1066); data from Bakolitsa et al. (Bakolitsa et al., 1999). Solvent-accessible surfaces of wild-type (wt) in A and mutant vinculin tail in B are coloured according to electrostatic potential, with basic patches in blue and acidic patches in red. The two lipid-binding sites (basic collar and basic ladder) are indicated by dotted lines. In mutant vinculin tail (B), point mutations of the C-terminus (CT) and helix 3 (H3) are circled. Vinculin mutants are referred to as CT and H3, and as lipid-binding-deficient mutant (LD) for the combination of both, respectively. (C) Pull-down assay to analyse the lipid-binding capacity of Vt mutants Vt(CT, H3, LD) and Vt(Δ1052), in comparison to the Vt wild type. Large unilamellar vesicles of the phospholipids PC, PS and PIP_2 were incubated with Vt proteins and sedimented. Pairs of pellet (P) and supernatant (S) fractions were detected on Coomassie-stained gels and analysed by densitometry. Columns represent the proportions of vesicle-bound Vt protein (means±s.e.; *n*=3). Notice the decreased binding of Vt mutants to acidic phospholipids. Average residual binding of all Vt proteins to pure PC vesicles is indicated (dashed line). Identical molar amounts of Vt protein were used for all assays. (D) The interaction of Vt proteins with Vh was analysed by GST pull-down assay. GST-Vh(D1) fusion protein bound to glutathione-Sepharose beads was incubated with Vt protein. Pellet fractions were analysed on Coomassie-stained gels. (E) Interaction of Vt mutants with actin filaments was analysed in a high-speed cosedimentation assay. Pellet and supernatant fractions were analysed by densitometry. Differences in actin binding between the Vt mutants were observed at a molar ration of actin:Vt of 2:1. Columns represent the proportions of actin-bound Vt protein (means±s.e.; *n*=3). (F) Expression of full-length GFP-vinculin in stably transfected B16-F1 mouse melanoma cells was compared with endogenous vinculin levels by western blotting (WB) using anti-vinculin antibodies. (G) Proportions of exogenous vinculin (means±s.e.; *n*=3).

the vinculin head-to-tail interface (Izard et al., 2004; Bakolitsa et al., 2004), and two residues R1060, K1061 in the C-terminal arm (Vt-CT mutant). In addition, we designed a Vt mutant in which all six residues were mutated – this is referred to as lipid binding deficient (Vt-LD). The reduction in charge density within the basic ladder and collar is visualized by modelling glutamines into the crystal structure of Vt instead of the respective arginines and lysines (Fig. 1B). Conservation of the α-helical structure in Vt-LD was confirmed by circular-dichroism spectroscopy (data not shown). We then tested the lipid-binding characteristics of bacterially expressed Vt (amino acids 858-1066) for the wild type and all three mutants in a cosedimentation assay, using SLVs. Vesicles were generated containing PC and the acidic phospholipids PS (45%) and PIP_2 (7%). This composition was chosen to mimic the lipid conditions at the inner leaflet of the plasma membrane (Niggli, 2001) during a local burst of PIP_2 production and to avoid electrostatic sequestration as a result of highly negatively charged surfaces that are characteristic of pure PIP_2 micelles or PS vesicles; as a control, pure PC vesicles were used. Binding of the wild-type construct Vt-wt to vesicles was compared with that of the C-terminal mutants Vt-Δ1052 (Bakolitsa et al., 1999) and Vt-CT (Ziegler et al., 2002), which had earlier been reported to display reduced phospholipid binding, and with that of the helix-3 mutant Vt-H3 and the putatively lipid-binding-deficient mutant Vt-LD. As shown in Fig. 1C, vesicle binding of the Vt mutants Vt-Δ1052, Vt-CT and Vt-H3 (with one site altered) led to a partial loss (more than 50%) in lipid binding, whereas the lipid-binding capacity of Vt-LD displayed a dramatic decrease of 80% compared with wild-type Vt. With the control PC vesicles, all Vt mutants behaved the same, displaying a basic value of ~16-20% of the maximal value seen for mixed-lipid-vesicle binding (Fig. 1C). Identical molar amounts of Vt protein were used for all assays shown in Fig. 1.

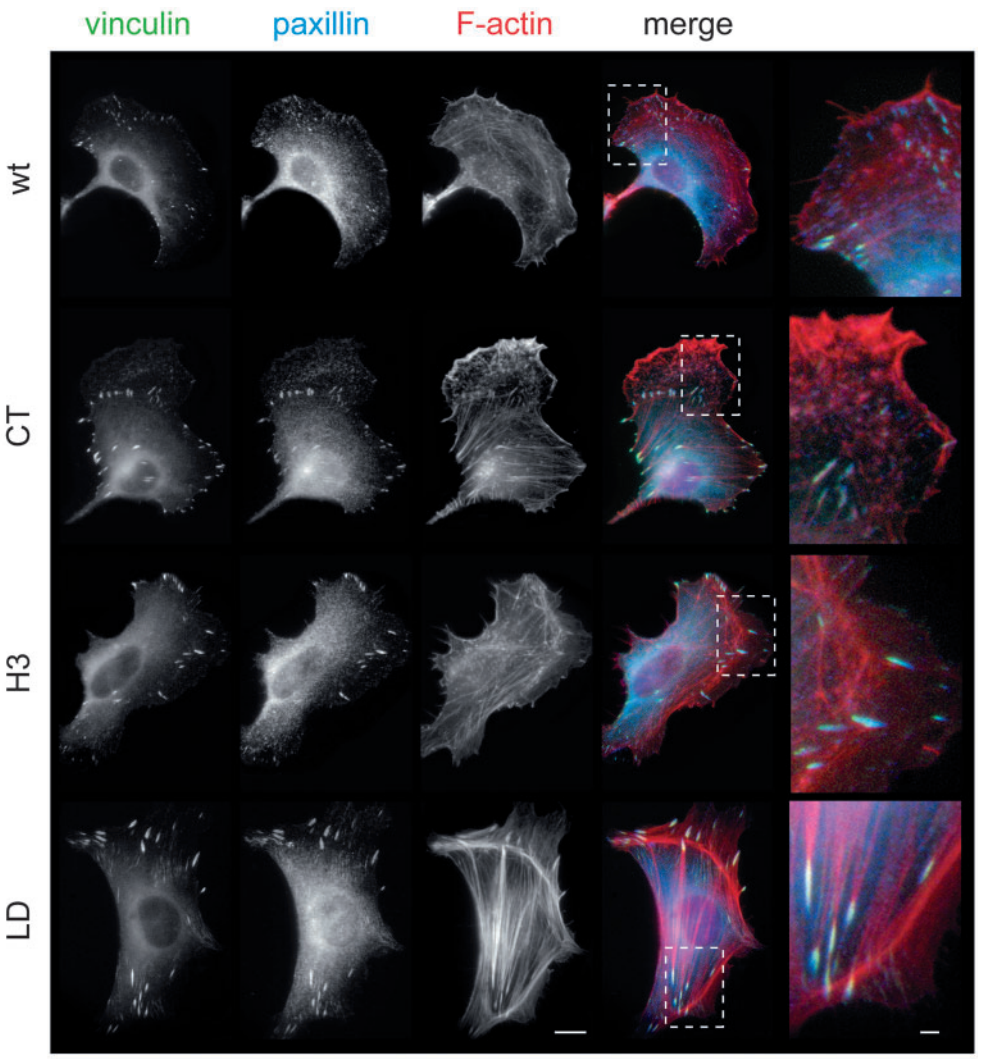

Fig. 2. Localization of GFP-vinculin constructs in B16-F1 cells. B16-F1 populations were seeded on laminin and allowed to attach for 6 hours. Thereafter, cells were fixed and stained for paxillin and the actin cytoskeleton. Localization of GFP-vinculin constructs, paxillin and F-actin in exemplary cells are shown individually (greyscale) as well as on merged images of GFP-vinculin (green), paxillin (blue), F-actin (red) and enlargements of the regions indicated. Scale bars, 10 μm (overviews); 2 μm (insets).

Vt mutants defective in lipid binding still bind protein ligands

The lipid-binding sites in helix 3 and the C-terminus overlap with attachment sites for protein ligands [e.g. for filamentous actin (Hüttelmaier et al., 1997) and for the vinculin head (Vh) (Izard et al., 2004; Miller et al., 2001)]. To analyse the consequences of the mutations described above on ligand binding, we performed a pull-down assay and a high-speed cosedimentation assay to probe for Vh or F-actin binding, respectively (Fig. 1D,E). Because the intramolecular head-to-tail interaction controls the ligand-binding properties of vinculin (Critchley, 2000; Bakolitsa et al., 2004), our vinculin mutants were designed to leave the head-to-tail interaction intact. In order to demonstrate this, we tested the interaction of Vt mutants with a GST-Vh [domain 1 (D1), 1-258] fusion protein. GST-Vh(D1) immobilized on glutathione-Sepharose beads was incubated with an excess of Vt protein and sedimented by centrifugation. As shown in Fig. 1D, the head-to-tail interaction was found to be functional for all Vt mutants. Cosedimentation with F-actin at a molar ratio of actin:Vt of 5:1 displayed >95% binding for all Vt mutants compared with

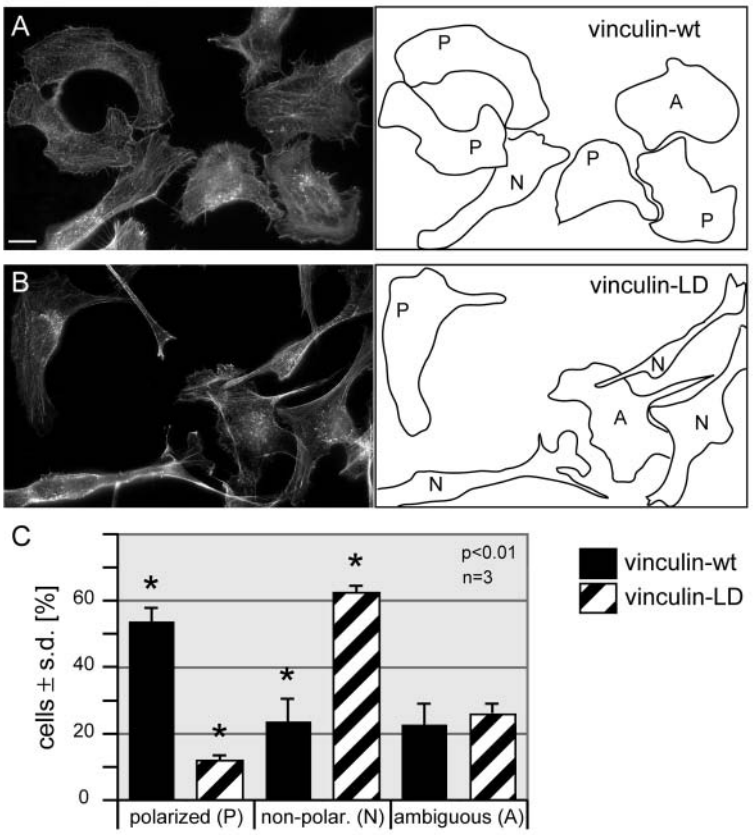

Fig. 3. Polarization of B16-F1 cells expressing vinculin variants. Populations expressing vinculin constructs were fixed 6 hours after seeding onto laminin and actin filaments stained using phalloidin. (A,B) Representative cells of populations expressing vinculin-wt (A) or vinculin-LD (B) are shown in fluorescence images (left) and as outlines of cells (right). Classification of cells into the categories polarized (P), unpolarized (N) and ambiguous (A) was based on cell shape and cytoskeletal staining. Scale bar, 10 μm. (C) Proportions of cells in each category taken from >600 cells (n=3 independent experiments) for each vinculin construct. Notice the significant difference between the numbers of polarized motile cells in the vinculin-wt-expressing B16-F1 and vinculin-LD-expressing cells.

wild-type Vt (data not shown), indicating that overall F-actin binding is well conserved. When a molar ratio of actin:Vt of 2:1 was used, a ratio that represents the maximal binding capacity of F-actin [0.3-0.5 moles of Vt per mole of actin (Johnson and Craig, 1995)], a decrease in binding of Vt mutants H3 and LD to 65% compared with the wild type was observed (Fig. 1E). In conclusion, the general conformation and overall binding specificities for protein ligands of the Vt domain were found to be largely intact in the lipid-binding-site mutants CT, H3 and LD.

Intracellular localization of vinculin variants is normal

B16-F1 mouse melanoma cells were transfected with full-length wild-type and mutant GFP-vinculin variants, and cell populations stably expressing the respective constructs were obtained by a combination of cell sorting and antibiotic selection. Expression of GFP-vinculin was stable for more than six passages. The resulting populations of cells expressing GFP-vinculin variants were used for a set of experiments to analyse alterations in protein localization, cell adhesion and migration. Protein expression patterns (Fig. 1F,G) were determined by semiquantitative western blotting of cell lysates from parental B16-F1 and transfected populations at different passages (1-5). A antibody against vinculin was used to monitor both endogenous vinculin and GFP fusion proteins (Fig. 1F). Comparison of the levels of recombinant to endogenous protein revealed ratios of exogenous to total vinculin varying from 0.3 to 0.45 (Fig. 1G). Cell populations stably expressing GFP-vinculin variants were generated several times with identical results.

Intracellular distribution patterns of GFP-vinculin fusion proteins in B16-F1 cells were analysed by counterstaining focal adhesions with anti-paxillin antibodies and actin filaments with phalloidin, in cells seeded onto laminin and fixed after 6 hours. Fig. 2 shows that wild-type GFP-vinculin as well as all lipid-binding mutants localized to focal adhesions, where they perfectly colocalized with paxillin to adhesion sites linked to actin filaments. The population of B16-F1 cells expressing GFP-vinculin-LD, however, displayed a high frequency of cells with abnormally long adhesive extensions. Furthermore, these cells contained more pronounced stress fibres and larger focal adhesions than populations expressing other vinculin variants (Fig. 2).

Vinculin-LD interferes with the motility of B16-F1 cells

On laminin, B16-F1 cells display a motile phenotype that is characterized by highly polarized cells with wide lamellipodia at their leading edges (Ballestrem et al., 1998). This phenotype was also observed in a large proportion of cells expressing vinculin-wt or vinculin mutants CT and H3 6 hours after attachment to laminin (see also Fig. 2). By contrast, the number of cells displaying this phenotype when expressing vinculin-LD was significantly reduced compared with cells expressing GFP-tagged vinculin-wt (Fig. 3A-C). Classification of more than 600 cells for each population allowed us to quantify the defect of vinculin-LD-expressing cells in adopting a motile phenotype. Whereas 54% of vinculin-wt cells displayed a motile phenotype and only 24% did not, this ratio was inverted in the vinculin-LD cells with 12% polarized and motile cells, whereas 63% of the cells were spread but not polarized or with clear lamellipodia and therefore judged to be non-motile. Using time-lapse microscopy of single cells migrating on laminin, locomotory activity of vinculin-wt-expressing cells was confirmed, whereas not a single motile vinculin-LD-expressing cell was detected in this assay (see Fig. S1 in supplementary material).

Vinculin-LD delays cell adhesion and spreading on different extracellular matrices

B16-F1 cells express receptors for the extracellular matrix proteins laminin (integrins $\alpha1\beta1$ and $\alpha6\beta1$), fibronectin (integrins $\alpha4\beta1$ and $\alpha5\beta1$) and collagen (integrin $\alpha1\beta1$) (Ballestrem et al., 1996). Hence, we tested the effect of our

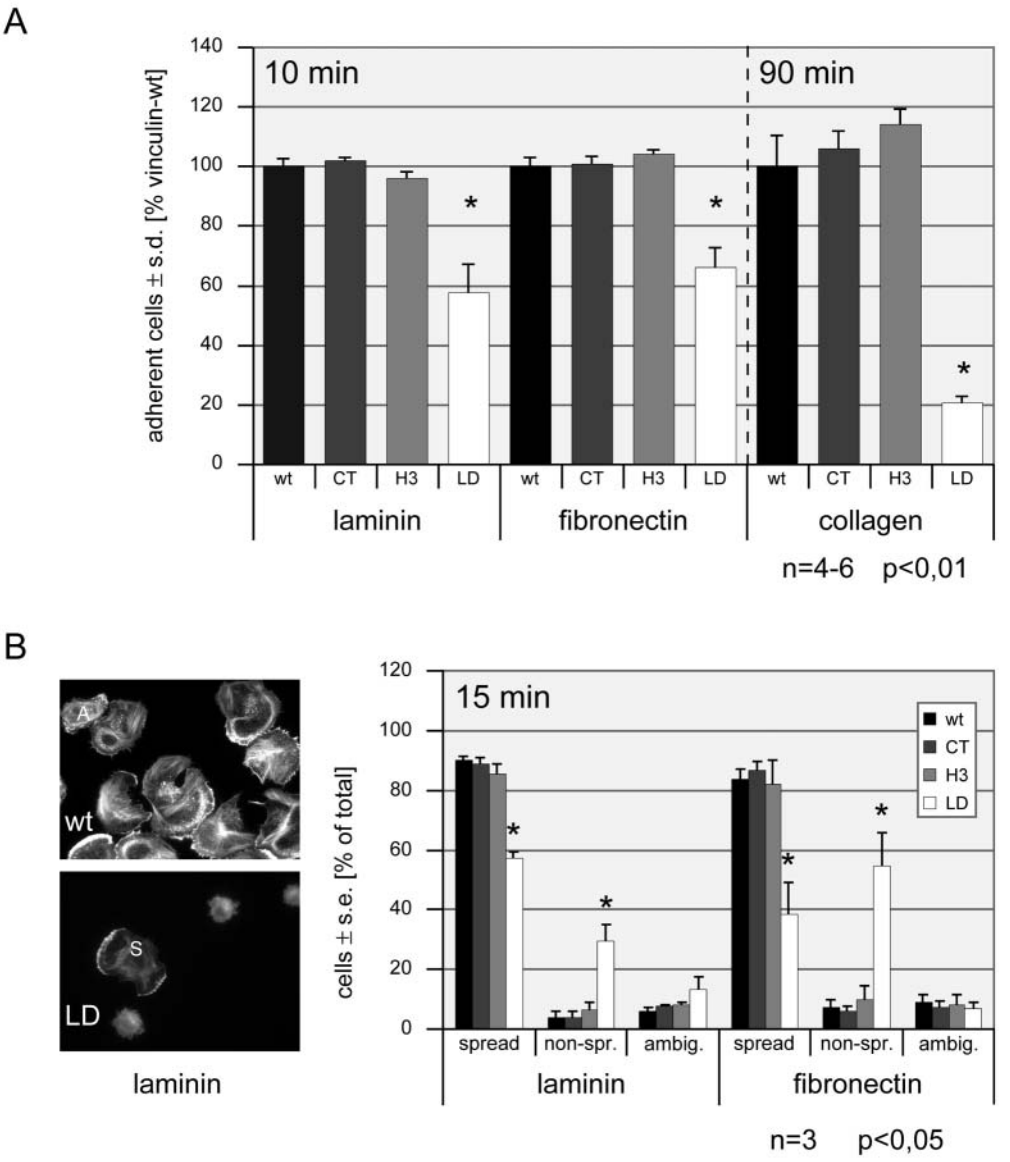

Fig. 4. Adhesion and spreading on different types of extracellular matrix. B16-F1 populations expressing different GFP-vinculin mutants were analysed on laminin, fibronectin and collagen. Identical numbers of cells were seeded onto 12-well plates coated with the matrix molecules. (A) Incubation times of 10 minutes on laminin and fibronectin, and 90 minutes on collagen, were chosen to obtain comparable cell adhesion. After washing and fixation, cells were counted and adhesion was quantified as a proportion of adherent cells (mean±s.d.; *n*=4-6) compared with adherent cells expressing the GFP-vinculin wild type. (B) To analyse spreading, cells were allowed to attach for 15 minutes on laminin or fibronectin and, after washing and fixation, stained with TRITC-phalloidin. Cells were classified into three groups: spread (S), non-spread (N) and ambiguous (A), as seen in cells expressing vinculin-wt or vinculin-LD. Depicted cells were scored as spread or non-spread, respectively, unless indicated otherwise. Spreading was quantified as a proportion of spread cells (mean±s.e.; *n*=3) compared with the total number of adherent cells.

vinculin variants for adhesion and spreading on these matrices. Populations of B16-F1 cells expressing wild-type or mutant GFP-vinculin were allowed to attach for various times. Comparable degrees of adhesion were reached on laminin and fibronectin 10 minutes after seeding, and on collagen after 90 minutes. Non-adherent cells were washed away and remaining cells counted in randomly selected microscopic fields. Cell adhesion was quantified as a proportion of adherent cells expressing the different vinculin variants (mean±s.d., *n*=4-6 independent experiments) compared with cells expressing GFP-vinculin-wt, using an average of 450-550 cells per test. As illustrated in Fig. 4A, vinculin-LD-expressing cells displayed a decrease in adhesion of 79% on collagen (after 90 minutes) and of 42% and 34% on laminin and fibronectin, respectively (after 10 minutes), compared with the vinculin-wt population.

To analyse the effects of vinculin variants on spreading, cells were allowed to attach for 15 minutes on laminin or fibronectin, fixed and phalloidin stained. Based on shape and cytoskeletal staining, cells were divided in three groups: spread, non-spread and ambiguous cells (Fig. 4B). Spreading was expressed as a proportion of spread cells compared with the total number of adherent cells (mean±s.e., *n*=3 independent experiments), using more than 150 cells per test. As illustrated in Fig. 4B, vinculin-LD-expressing cells displayed a decrease in spreading of 31% and 46% on laminin and fibronectin, respectively (after 15 minutes), and six times more non-spread cells than cells expressing vinculin-wt or other vinculin variants. After 90 minutes of adhesion and spreading on laminin or fibronectin, differences in the number of adherent cells were decreased to less than 10%. Therefore, we conclude that vinculin-LD induces a delay in cell spreading compared with the other vinculin constructs rather than a defect in adhesion.

Vinculin-LD strongly impairs the migration of B16-F1 cells in collagen gels

Spontaneous migration of cells expressing mutant and wild-type GFP-vinculin was analysed in a three-dimensional collagen

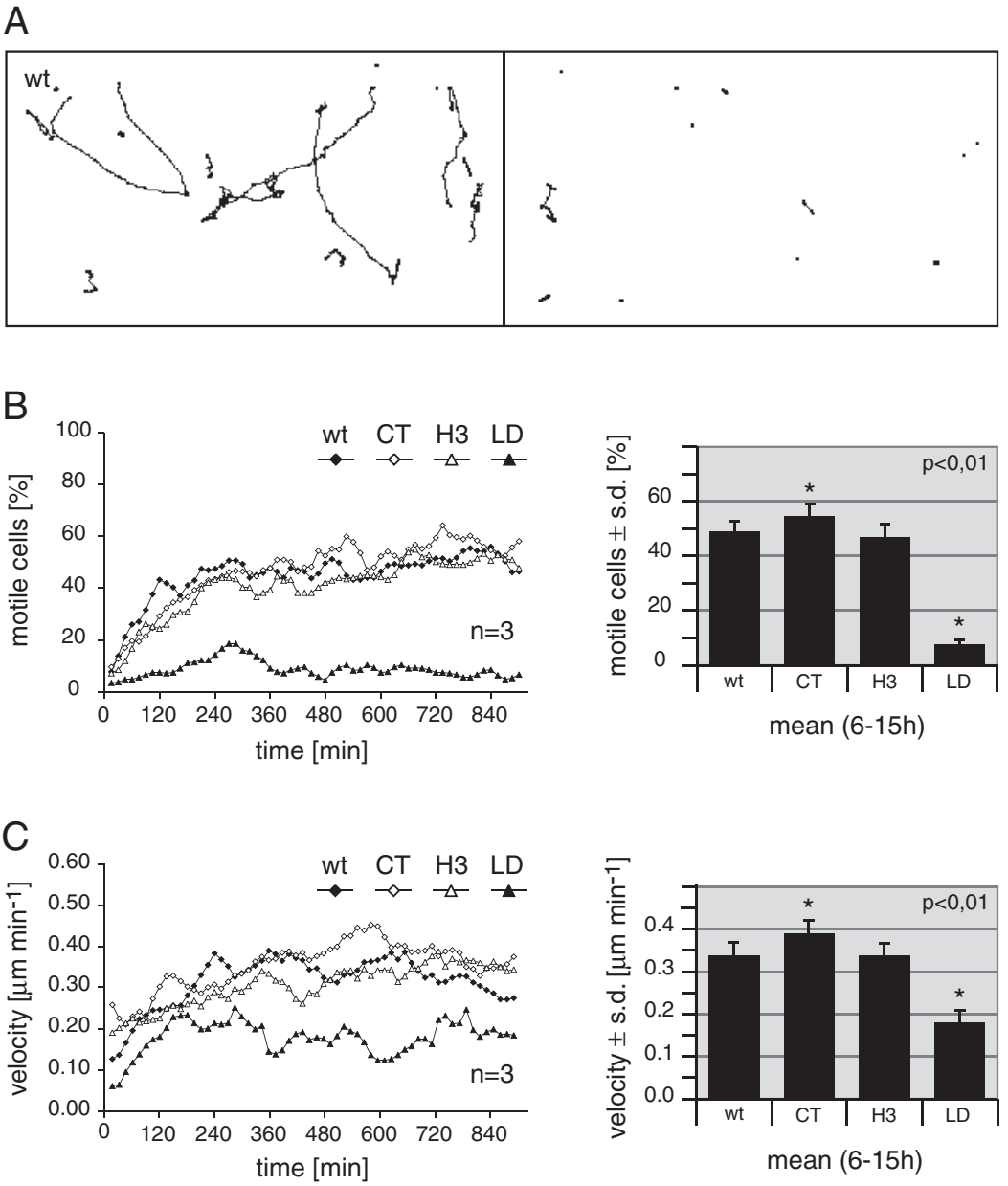

Fig. 5. Locomotory activity and velocity of B16-F1 populations in collagen gels. Migration of B16-F1 cells expressing vinculin variants was analysed by time-lapse video microscopy. The number and velocity of motile cells were calculated from tracking data (30 cells per vinculin variant, *n*=3 repeats). (A) Representative tracks of cells expressing vinculin-wt or vinculin-LD, respectively. Columns represent (B) average of motile cells (mean±s.d.) and (C) average velocity of active cells (mean±s.d.) of the population between 6-15 hours (constant phase).

matrix. The cells were embedded in collagen and migration of cells (*n*=30) in one field was followed for 15 hours using time-lapse video microscopy. Differences in motility of vinculin-wt- and vinculin-LD-expressing cells became immediately evident upon comparison of representative tracks (Fig. 5A). Both the proportion of motile cells and their velocity were calculated from tracking data (Fig. 5B,C). After an initial phase of adhesion to the collagen matrix (also compare to spreading, Fig. 4), the number of motile cells remained constant and averages (mean±s.d.) were calculated for each of the populations between 6 hours and 15 hours (constant phase). A reduction of motility to 16% compared with the wild type (and other vinculin constructs) was observed in the vinculin-LD-expressing cell population (Fig. 5B). The velocity was determined from the relative movement of motile cells (Fig. 5C). During the constant phase of movement (6-15 hours), the average velocity (mean±s.d.) of vinculin-LD-expressing cells was reduced to 53% of the value of cells expressing exogenous vinculin-wt, revealing a strong inhibition of cell migration. This effect was observed on a background of endogenous vinculin (70% of total vinculin, also compare to Fig. 1F). The persistence of cell migration was analysed based on angle changes, showing no significant differences (data not shown). Values for vinculin-LD, however, were calculated based on a few rather short tracks, because most cells registered did not migrate at all.

Vinculin-LD is correctly incorporated into adhesion sites but inhibits translocation and disassembly of adhesions

Localization of vinculin-LD was indistinguishable from that of vinculin-wt in B16-F1 cells, but the number of stress fibres and the number and size of adhesions appeared to be increased in vinculin-LD-expressing cells (see also Fig. 2). To test whether exchange rates of vinculin molecules in individual adhesion sites are altered in vinculin-LD-expressing cells, we used FRAP to measure the rate of re-incorporation of GFP-tagged

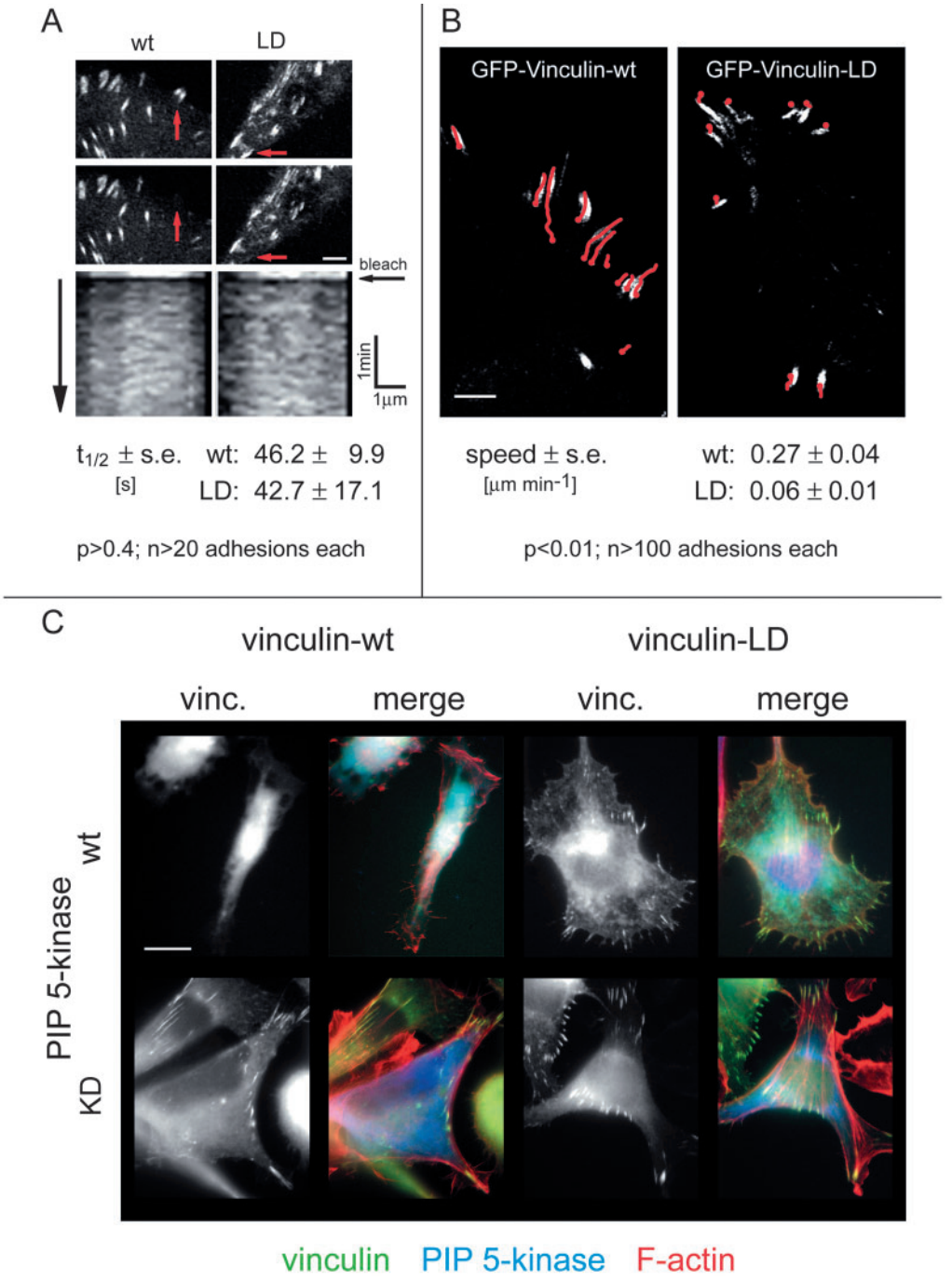

Fig. 6. Adhesion-site dynamics and PIP_2 signals. In B16-F1 cells expressing GFP-vinculin variants, individual adhesions were analysed using confocal laser-scanning microscopy. (A) Representative images of adhesions before and after bleaching (red arrows) and kymographs from line scans parallel to the length axis of bleached adhesion. The half-time of fluorescence recovery was calculated based on the kymographs. Notice that vinculin variants wt and LD have comparable incorporation rates. Scale bar, 5 μm. (B) Movement of adhesions was followed over 20 minutes. Representative areas of cells expressing vinculin-wt or vinculin-LD are given, showing start position of adhesions (t=0 minutes) and tracks of adhesions tips marked in red (t=0-20 minutes). Tracks were used to calculate the average speed of retrograde movement. Scale bar, 5 μm. (C) B16-F1 cells were seeded onto fibronectin, transfected with murine PIP 5-kinase α, wild type (wt) or kinase deficient (KD), and fixed 12 hours after transfection. Localization of GFP-vinculin variants (wt or LD) is shown individually (greyscale, left) and in merged images (green) together with PIP 5-kinase α (blue) and F-actin (red). Scale bar, 10 μm. Notice that only cells expressing wild-type constructs of both PIP 5-kinase and vinculin show a localization of vinculin that is entirely perinuclear and start to detach.

vinculin variants after bleaching. The half-time of fluorescence recovery after photobleaching was about 45 seconds for both wild-type and lipid-binding-deficient vinculins (Fig. 6A) in adhesions that remained stable for more than 10 minutes. Hence, a lipid-binding deficiency of vinculin-LD does not interfere with its incorporation into and exchange rate for individual adhesion sites. To study further the impairment of cell migration in vinculin-LD-expressing cells (Figs 3, 5), we then analysed the overall turnover of adhesion sites. Confocal video microscopy of individual adhesions revealed a strong inhibition of retrograde sliding (translocation) in vinculin-LD-expressing cells (Fig. 6B). To estimate the average speed of adhesion-site movement towards the cell centre, more than 100 individual sites per vinculin variant were tracked. Adhesions in vinculin-LD-expressing B16-F1 cells translocated at 22% of the speed acquired by vinculin-wt-expressing cells, reflecting a prominent stabilization of adhesion sites by vinculin-LD. The influence of vinculin-LD on adhesion stability was further emphasized by the finding that the number of adhesion sites formed and disassembled during the observation period of 20 minutes was remarkably different from controls. In vinculin-wt-expressing cells, 27% of total adhesions were newly formed and 32% were disassembled, whereas only 9% were formed and 2% disassembled in cells expressing vinculin-LD. Thus, vinculin-wt-expressing cells showed a five times higher adhesion-site turnover than cells expressing the lipid-binding-

deficient mutant. Hence, we conclude that cell signalling leading to turnover of adhesion sites requires the ability of vinculin to bind acidic phospholipids, whereas the basic exchange rates of vinculin molecules for a given adhesion (i.e. during adhesion-site maintenance) do not.

Our results argue strongly for a lipid-dependent regulation of vinculin interactions in adhesion sites (Fig. 7). To test this model further, we asked whether a general increase in cellular PIP_2 levels could trigger the release of vinculin from adhesions and whether this might be altered in vinculin-LD-expressing cells. We therefore overexpressed murine PIP 5-kinase α (Tolias et al., 2000), which leads to membrane localization of this kinase and high PIP_2 levels (Doughman et al., 2003), in B16-F1 cells co-expressing either the vinculin-wt or the vinculin-LD variant. In line with our model, increased PIP_2 levels in these cells induced relocalization of vinculin-wt from adhesion sites to the perinuclear region. This effect was evident 8 hours after transfection of B16-F1 cells (data not shown). By 12 hours, cells expressing PIP 5-kinase α had lost vinculin-wt staining from adhesion sites and started to detach (Fig. 6C). By contrast, cells expressing GFP-vinculin-LD were more resistant to this treatment. Out of 60 cells co-expressing vinculin-LD and PIP 5-kinase α for 12 hours, 41 showed vinculin-LD localized to adhesion sites (Fig. 6C). Moreover, the effect of PIP-5-kinase-α overexpression was dependent on the enzymatic activity of PIP 5-kinase α and is contrast with that of PIP 5-kinase γ, which also displaces talin as a kinase-dead variant (Ling, 2002), not competing with vinculin binding to adhesion sites. Thus, in cells expressing kinase-deficient (KD) PIP 5-kinase α (Shibasaki et al., 1997), no relocalization was observed of vinculin-wt or -LD (Fig. 6C), indicating that lipid-kinase activity was required to displace vinculin from adhesions. These findings support the view that the connection between integrin-based adhesions and the actin cytoskeleton is regulated by PIP_2 signals in a vinculin-dependent fashion.

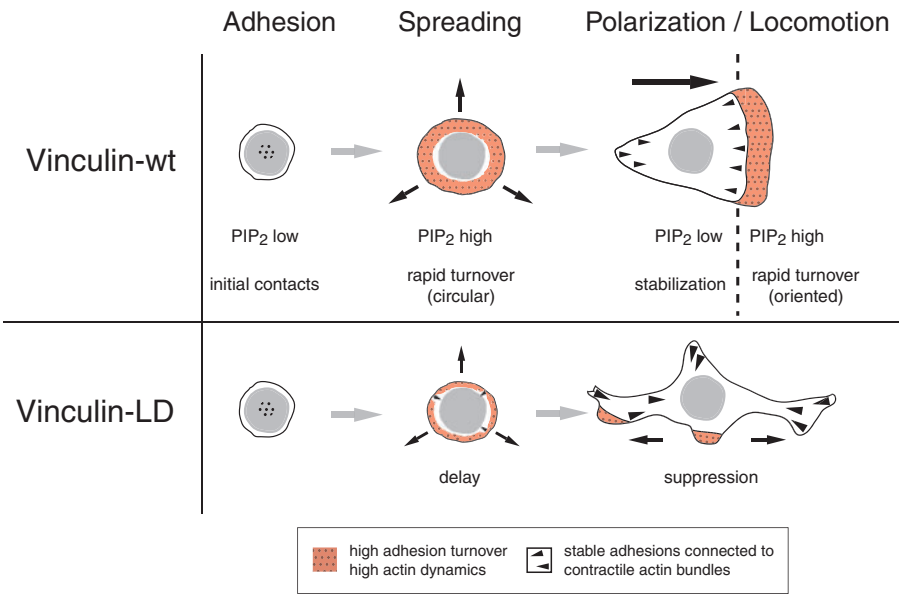

Fig. 7. Model of vinculin involvement in the regulation of adhesion turnover. In motile cells, areas with both high adhesion turnover and high actin dynamics under the control of the small GTPase Rac depend on elevated PIP_2 levels, which leads to a weakening of the interaction of vinculin-containing adhesions with actin filaments. When acidic phospholipid binding to vinculin is defective, adhesion sites are stabilized and efficient progression of lamellipodia is impaired. This leads to a delay in cell spreading and an almost complete inhibition of cell motility in vinculin-LD-expressing cells.

Discussion

Among the large catalogue of adhesion proteins, many bind to and seem to be regulated by acidic phospholipids (Niggli, 2001), but the precise consequences of this process for cell adhesion and motility are still an enigma. In the study presented here, we analysed the functional significance of PIP_2 binding to vinculin, a prominent structural component of adhesion sites. An increasing body of evidence indicates that vinculin is involved in the stabilization of nascent cell-matrix adhesions after binding of talin to integrins (Galbraith et al., 2002; Giannone et al., 2003; Zaidel-Bar et al., 2003). This process, requiring activation and recruitment of vinculin, is apparently independent of the vinculin-PIP_2 interaction, as shown here. The GFP-tagged mutants of vinculin used (H3, CT and LD) target newly formed adhesion sites within lamellipodia, where they co-localize with paxillin. They are also recruited to mature focal adhesions at the ventral side of the cell body and the trailing edge. In addition, the incorporation of GFP-vinculin-LD into adhesions is not reduced in comparison to the vinculin-wt variant, as shown by FRAP analysis of incorporation rates. We thus conclude that recruitment of vinculin during reinforcement or maturation of adhesion sites does not depend on the capacity of vinculin to bind acidic phospholipids such as PIP_2. This is consistent with preliminary reports from other groups, who observed that different mutants in the lipid-binding sites of the vinculin tail did not significantly affect subcellular vinculin localization (Saunders et al., 2003; Cohen and Craig, 2003), except for one C-terminal deletion mutant (Bakolitsa et al., 1999) in which the last 15 amino acids were removed. The localization of this vinculin mutant was altered from peripheral focal adhesions to a more fibrillar distribution (Saunders et al., 2003). This distribution might reflect a destabilization of the helix bundle in Vt and subsequent partial unfolding of the protein (Bakolitsa et al., 1999). By contrast, our vinculin-LD mutant led to the pronounced formation of large mature adhesion sites linked to stress fibres. Our GFP-tagged vinculin constructs were expressed in the presence of endogenous vinculin; therefore, localization to focal adhesions could be guided through formation of vinculin hetero-oligomers. However, when expressed in vinculin (–/–) MEF cells (Xu et al., 1998a), vinculin-LD still localized to focal adhesions (R. Saunders and D. Critchley, personal communication; I.C. and W.H.Z., unpublished). Hence, recruitment of vinculin-LD to adhesion sites is independent not only of phospholipid binding but also of the presence of endogenous vinculin in adhesion

sites. Possibly, vinculin-LD molecules are activated and retained in adhesion sites by their interaction with talin and further ligands.

Spreading of cells requires a high turnover of small, transient adhesion sites to allow (fast) outward movement of peripheral lamellipodia under the control of the small Rho-family GTPase Rac (Rottner et al., 1999b; Sheetz et al., 1999). The spreading process is independent of force coupling to talin (Giannone et al., 2003) and RhoA-controlled actomyosin contractility (Zaidel-Bar et al., 2003), two mechanisms that are involved in adhesion-site maturation (Giannone et al., 2003; Rottner et al., 1999b). By contrast, spreading depends on non-receptor tyrosine kinases such as focal-adhesion kinase (FAK) and Src-family kinases (Von Wichert et al., 2003). Tyrosine kinases are activated as a result of integrin binding to the extracellular matrix (Felsenfeld et al., 1999; Wang et al., 2001). In addition, tyrosine phosphorylation is a hallmark of adhesion sites (Zaidel-Bar et al., 2003) and tight control of phosphorylation regulates the function of cytoskeletal proteins during cell spreading. For instance, in protein-tyrosine-phosphatase-2-deficient fibroblasts, FAK activity strongly reduces the residence lifetime of paxillin and vinculin in adhesion sites (Von Wichert et al., 2003). Protein-tyrosine-phosphatase-2 deficiency leads to inhibition of cell spreading on fibronectin and vitronectin, as well as to the accumulation of immature adhesions lacking α-actinin (Von Wichert et al., 2003). Effects of tyrosine kinase activity on vinculin recruitment to adhesion sites were also observed for cell adhesion to vitronectin, because vinculin is only recruited to force-activated vitronectin receptors in c-Src-deficient cells (Felsenfeld et al., 1999; Galbraith et al., 2002). Both examples suggest that tyrosine-kinase activity can negatively regulate the association of vinculin and paxillin with adhesion sites, leading to increased adhesion dynamics. This conclusion is further supported by the behaviour of vinculin-deficient fibroblasts, which show reduced spreading and less-stable focal adhesions accompanied by an increase in FAK activity and in locomotion (Xu et al., 1998a).

From these findings, it can be concluded that lack of vinculin inhibits cell spreading owing to a disability of the affected cells to stabilize initial adhesions. This mechanism cannot, however, explain the severe spreading defect observed in vinculin-LD-expressing B16-F1 cells (this study), because these cells produce mature adhesion sites and display a strongly reduced migratory activity associated with a severely diminished movement of individual adhesion sites. The defect in spreading of B16-F1 cells does not result from a reduced speed of incorporation of the mutant vinculin and is observed in the presence of endogenous vinculin. Combining these observations with data showing that PIP_2 and actin binding to the vinculin tail can compete with each other (Steimle et al., 1999), and with our results showing that the actin-binding ability of Vt-LD seems largely intact, we propose that incorporation of vinculin-LD into newly formed adhesion sites leads to an interaction with F-actin but does not respond to release signals from the cell membrane. Subsequently, an unregulated interaction between integrins and the actin cytoskeleton prevents the rapid turnover of adhesion sites, as would be required for cell spreading and in lamellipodia of migrating cells (Fig. 7). Furthermore, vinculin acts as a scaffold for other adhesion proteins (Critchley, 2000) and these complexes might also be stabilized by the LD mutant.

Residence-lifetime analysis of vinculin in adhesion sites has shown that the half-time of recovery for GFP-vinculin is considerably shorter than overall lifetimes of adhesions in B16-F1 cells (this study). A similar relation between lifetimes was reported in fibroblasts (Von Wichert et al., 2003). Because the vinculin exchange rates within adhesion sites must be such that the protein can balance the stabilization and maturation of adhesions against dissipation, vinculin can contribute to a differential control of adhesion-site assembly and disassembly, as observed at different locations in motile cells (Ballestrem et al., 2001; Von Wichert et al., 2003; Wehrle-Haller and Imhof, 2002). This control function is rendered inadequate by introducing a dominant negative mutant of vinculin that is incapable of transducing PIP_2 signals to the destabilization of the adhesion structure.

In contrast to a previous report (Gilmore and Burridge, 1996), we did not find evidence for a PIP_2-binding-dependent incorporation of vinculin into focal adhesions. Instead, our results are consistent with the assumption that vinculin acts as a sensor, thus converting local modulation of PIP_2 levels to adhesion-site dynamics. Vinculin-LD is unable to execute this function. Finally, PIP_2 might also influence the association of vinculin binding partners other than talin and F-actin like the actin-nucleator complex Arp2/3 (DeMali et al., 2002) and protein kinase Cα (Ziegler et al., 2002).

We are grateful to S. Hüttelmaier for the vinculin-encoding cDNA, L. Machesky for PIP 5-kinase α and L61-Rac expression constructs, L. Gröbe for cell sorting, J. Kuper and W.-D. Schubert for help with the graphical representation of vinculin, and E. Saxinger and B. Mainusch for excellent technical assistance. We thank D. R. Critchley and K. Rottner for helpful discussions. This work was supported by grants from the German Research Council (DFG) to W.H.Z., B.M.J. and T.E.B.S., the Fonds der Chemischen Industrie (to W.H.Z. and B.M.J.) and Land Niedersachsen (scholarship to I.C.).

References

Bakolitsa, C., de Pereda, J. M., Bagshaw, C. R., Critchley, D. R. and Liddington, R. C. (1999). Crystal structure of the vinculin tail suggests a pathway for activation. *Cell* **99**, 603-613.

Bakolitsa, C., Cohen, D. M., Bankston, L. A., Bobkov, A. A., Cadwell, G. W., Jennings, L., Critchley, D. R., Craig, S. W. and Liddington, R. C. (2004). Structural basis for vinculin activation at sites of cell adhesion. *Nature* **430**, 583-586.

Ballestrem, C. G., Uniyal, S., McCormick, J. I., Chau, T., Singh, B. and Chan, B. M. (1996). VLA-beta 1 integrin subunit-specific monoclonal antibodies MB1.1 and MB1.2: binding to epitopes not dependent on thymocyte development or regulated by phorbol ester and divalent cations. *Hybridoma* **15**, 125-132.

Ballestrem, C., Wehrle-Haller, B. and Imhof, B. (1998). Actin dynamics in living mammalian cells. *J. Cell Sci*. **111**, 1649-1658.

Ballestrem, C., Hinz, B., Imhof, B. A. and Wehrle-Haller, B. (2001). Marching at the front and dragging behind: differential alphaVbeta3-integrin turnover regulates focal adhesion behavior. *J. Cell Biol*. **155**, 1319-1332.

Barret, C., Roy, C., Montcourrier, P., Mangeat, P. and Niggli, V. (2000). Mutagenesis of the phosphatidylinositol 4,5-bisphosphate (PIP_2) binding site in the NH_2-terminal domain of ezrin correlates with its altered cellular distribution. *J. Cell Biol*. **151**, 1067-1080.

Bass, M. D., Patel, B., Barsukov, I. G., Fillingham, I. J., Mason, R., Smith, B. J., Bagshaw, C. R. and Critchley, D. R. (2002). Further characterization of the interaction between the cytoskeletal proteins talin and vinculin. *Biochem. J*. **362**, 761-768.

Borgon, R. A., Vonrhein, C., Bricogne, G., Bois, P. R. J. and Izard, T. (2004). Crystal structure of human vinculin. *Structure* **12**, 1189-1197.

Calderwood, D. A., Yan, B., De Pereda, J. M., Alvarez, B. G., Fujioka, Y., Liddington, R. C. and Ginsberg, M. H. (2002). The phosphotyrosine binding-like domain of talin activates integrins. *J. Biol. Chem*. **277**, 21749-21758.

Caroni, P. (2001). Actin cytoskeleton regulation through modulation of PI(4,5)P_2 rafts. *EMBO J.* **20**, 4332-4336.
Cohen, D. M. and Craig, S. W. (2003). A cell-free system to investigate the role of inositol phospholipids in vinculin recruitment to focal adhesions. *Mol. Biol. Cell* **14**, 63a.
Critchley, D. R. (2000). Focal adhesions – the cytoskeletal connection. *Curr. Opin. Cell Biol.* **12**, 133-139.
DeMali, K. A., Barlow, C. A. and Burridge, K. (2002). Recruitment of the Arp2/3 complex to vinculin: coupling membrane protrusion to matrix adhesion. *J. Cell Biol.* **159**, 881-891.
DiPaolo, G., Pellegrini, L., Letinic, K., Cestra, G., Zoncu, R., Voronov, S., Chang, S., Guo, J., Wenk, M. R. and De Camilli, P. (2002). Recruitment and regulation of phosphatidylinositol phosphate kinase type 1gamma by the FERM domain of talin. *Nature* **420**, 85-89.
Doughman, R. L., Firestone, A. J. and Anderson, R. A. (2003). Phosphatidylinositol phosphate kinases put PI4,5P_2 in its place. *J. Membr. Biol.* **194**, 77-89.
Felsenfeld, D. P., Schwartzberg, P. L., Venegas, A., Tse, R. and Sheetz, M. P. (1999). Selective regulation of integrin-cytoskeleton interactions by the tyrosine kinase Src. *Nat. Cell Biol.* **1**, 200-206.
Fraley, T. S., Tran, T. C., Corgan, A. M., Nash, C. A., Hao, J., Critchley, D. R. and Greenwood, J. A. (2003). Phosphoinositide binding inhibits alpha-actinin bundling activity. *J. Biol. Chem.* **278**, 24039-24045.
Galbraith, C. G., Yamada, K. M., and Sheetz, M. P. (2002). The relationship between force and focal complex development. *J. Cell Biol.* **159**, 695-705.
Garcia-Alvarez, B., de Pereda, J. M., Calderwood, D. A., Ulmer, T. S., Critchley, D. R., Campbell, I. D., Ginsberg, M. H. and Liddington, R. C. (2003). Structural determinants of integrin recognition by talin. *Mol. Cell* **11**, 49-58.
Giannone, G., Jiang, G., Sutton, D. H., Critchley, D. R. and Sheetz, M. P. (2003). Talin1 is critical for force-dependent reinforcement of initial integrin-cytoskeleton bonds but not tyrosine kinase activation. *J. Cell Biol.* **163**, 409-419.
Gilmore, A. P. and Burridge, K. (1996). Regulation of vinculin binding to talin and actin by phosphatidyl-inositol-4,5-bisphosphate. *Nature* **381**, 531-535.
Hüttelmaier, S., Bubeck, P., Rudiger, M. and Jockusch, B. M. (1997). Characterization of two F-actin-binding and oligomerization sites in the cell-contact protein vinculin. *Eur. J. Biochem.* **247**, 1136-1142.
Hüttelmaier, S., Mayboroda, O., Harbeck, B., Jarchau, T., Jockusch, B. M. and Rudiger, M. (1998). The interaction of the cell-contact proteins VASP and vinculin is regulated by phosphatidylinositol-4,5-bisphosphate. *Curr. Biol.* **8**, 479-488.
Izard, T., Evans, G., Borgon, R. A., Rush, C. L., Bricogne, G. and Bois, P. R. (2004). Vinculin activation by talin through helical bundle conversion. *Nature* **427**, 171-175.
Jiang, G., Giannone, G., Critchley, D. R., Fukumoto, E. and Sheetz, M. P. (2003). Two-picoNewton slip bond between fibronectin and the cytoskeleton depends on talin. *Nature* **424**, 334-337.
Johnson, R. P. and Craig, S. W. (1995). F-Actin binding site masked by the intramolecular association of vinculin head and tail domains. *Nature* **373**, 261-264.
Lamarche, N., Tapon, N., Stowers, L., Burbelo, P. D., Aspenstrom, P., Bridges, T., Chant, J. and Hall, A. (1996). Rac and Cdc42 induce actin polymerisation and G1 cell cycle progression independently of $p65^{PAK}$ and the JNK/SAPK MAP kinase cascade. *Cell* **87**, 519-529
Ling, K., Doughman, R. L., Firestone, A. J., Bunce, M. W. and Anderson, R. A. (2002). Type I gamma phosphatidylinositol phosphate kinase targets and regulates focal adhesions. *Nature* **420**, 89-93.
Martel, V., Racaud-Sultan, C., Dupe, S., Marie, C., Paulhe, F., Galmiche, A., Block, M. R. and Albiges-Rizo, C. (2001). Conformation, localization and integrin-binding of talin depend on its interaction with phosphoinositides. *J. Biol. Chem.* **276**, 21217-21227.
Miller, G. J., Dunn, S. D. and Ball, E. H. (2001). Interaction of the N- and C-terminal domains of vinculin. Characterization and mapping studies. *J. Biol. Chem.* **276**, 11729-11734.
Nayal, A., Webb, D. J. and Horwitz, A. F. (2004). Talin: an emerging focal point of adhesion dynamics. *Curr. Opin. Cell Biol.* **16**, 1-5.
Niggemann, B., Maaser, K., Lu, H., Kroczek, K. S., Zanker, R. and Friedl, P. (1997). Locomotory phenotypes of human tumor cell lines and T lymphocytes in a three-dimensional collagen lattice. *Cancer Lett.* **118**, 173-180.
Niggli, V. (2001). Structural properties of lipid-binding sites in cytoskeletal proteins. *Trends Biochem. Sci.* **26**, 604-611.
Papagrigoriou, E., Gingras, A. R., Barsukov, I. L., Bate, N., Fillingham, I. J., Frank, R., Ziegler, W. H., Roberts, G. C. K., Critchley, D. R. and Emsley, J. (2004). Activation of a vinculin binding site in the talin rod involves re-arrangement of a five helix bundle. *EMBO J.* **23**, 2943-2951.
Pollard, T. D. and Borisy, G. G. (2003). Cellular motility driven by assembly and disassembly of actin filaments. *Cell* **112**, 453-465.
Ridley, A. J., Schwartz, M. A., Burridge, K., Firtel, R. A., Ginsberg, M. H., Borisy, J. T., Parsons, G. and Horwitz, A. R. (2003). Cell migration: integrating signals from front to back. *Science* **302**, 1704-1709.
Rodriguez Fernandez, J. L., Geiger, B., Salomon, D. and Ben-Ze'ev, A. (1992). Overexpression of vinculin suppresses cell motility in BALB/c 3T3 cells. *Cell. Motil. Cytoskeleton* **22**, 127-134.
Rodriguez Fernandez, J. L., Geiger, B., Salomon, D. and Ben-Ze'ev, A. (1993). Suppression of vinculin expression by antisense transfection confers changes in cell morphology, motility, and anchorage-dependent growth of 3T3 cells. *J. Cell Biol.* **122,** 1285-1294.
Rottner, K., Behrendt, B., Small, J. V. and Wehland, J. (1999a). VASP dynamics during lamellipodia protrusion. *Nat. Cell Biol.* **1**, 321-322.
Rottner, K., Hall, A. and Small, J. V. (1999b). Interplay between Rac and Rho in the control of substrate contact dynamics. *Curr. Biol.* **9**, 640-648.
Rozelle, A. L., Machesky, L. M., Yamamoto, M., Driessens, M., Hinsall., R. H., Roth, M. G., Luby-Phelps, K., Marriott, G., Hall, A. and Yin, H. L. (2000). Phosphatidylinositol 4,5-bisphosphate induces actin-based movement of raft-enriched vesicles through WASP-Arp2/3. *Curr. Biol.* **10**, 311-320.
Rüdiger, M., Jockusch, B. M. and Rothkegel, M. (1997). Epitope tag-antibody combination useful for the detection of protein expression in prokaryotic and eukaryotic cells. *BioTechniques* **23**, 96-97.
Saunders, R., Jennings, L., Sutton, D. H., Barsukov, I., Holt, M. R., Dunn, G. A., Adamson, E. D. and Critchley, D. R. (2003). Vinculin mutations that decrease PIP2 binding lead to protein mislocalisation and failure to rescue cell spreading defects in vinculin null fibroblasts. *Mol. Biol. Cell* **14**, 63a.
Sechi, A. S. and Wehland, J. (2000). The actin cytoskeleton and plasma membrane connection: PtdIns(4,5)P_2 influences cytoskeletal protein activity at the plasma membrane. *J. Cell Sci.* **113**, 3685-3695.
Sheetz, M. P., Felsenfeld, D., Galbraith, C. G. and Choquet, D. (1999). Cell migration as a five-step cycle. *Biochem. Soc. Symp.* **65**, 233-243.
Shibasaki, Y., Ishihara, H., Kizuki, N., Asano, T., Oka, Y. and Yazaki, Y. (1997). Massive actin polymerisation induced by phosphatidylinositol-4-phosphate 5-kinase in vivo. *J. Biol. Chem.* **272**, 7578-7581.
Steimle, P. A., Hoffert, J. D., Adey, N. B. and Craig, S. W. (1999). Polyphosphoinositides inhibit the interaction of vinculin with actin filaments. *J. Biol. Chem.* **274**, 18414-18420.
Tadokoro, S., Shattil, S. J., Eto, K., Tai, V., Liddington, R. C., de Pereda, J. M., Ginsberg, M. H. and Calderwood, D. A. (2003). Talin binding to integrin beta tails: a final common step in integrin activation. *Science* **302**, 103-106.
Tolias, K. F., Hartwig, J. H., Ishihara, H., Shibasaki, Y., Cantley, L. C. and Carpenter, C. L. (2000). Type I alpha phosphatidylinositol-4-phosphate 5-kinase mediates Rac-dependent actin assembly. *Curr. Biol.* **10**, 153-156.
Von Wichert, G., Haimovich, B., Feng, G. S. and Sheetz, M. P. (2003). Force-dependent integrin-cytoskeleton linkage formation requires downregulation of focal complex dynamics by Shp2. *EMBO J.* **22**, 5023-5035.
Wang, H. B., Dembo, M., Hanks, S. K. and Wang, Y. (2001). Focal adhesion kinase is involved in mechanosensing during fibroblast migration. *Proc. Natl. Acad. Sci. USA* **98**, 11295-11300.
Weekes, J., Barry, S. T. and Critchley, D. R. (1996). Acidic phospholipids inhibit the intramolecular association between the N- and C-terminal regions of vinculin, exposing actin-binding and protein kinase C phosphorylation sites. *Biochem. J.* **314**, 827-832.
Wehrle-Haller, B. and Imhof, B. (2002). The inner lives of focal adhesions. *Trends Cell Biol.* **12**, 382-389.
Wessel, D. and Flügge, U. I. (1984). A method for the quantitative recovery of protein in dilute solution in the presence of detergents and lipids. *Anal. Biochem.* **138**, 141-143.
Xu, W., Baribault, H. and Adamson, E. D. (1998a). Vinculin knockout results in heart and brain defects during embryonic development. *Development* **125**, 327-337.
Xu, W., Coll, J. L. and Adamson, E. D. (1998b). Rescue of the mutant phenotype by reexpression of full-length vinculin in null F9 cells; effects on cell locomotion by domain deleted vinculin. *J. Cell Sci.* **111**, 1535-1544.
Yin, H. L. and Janmey, P. A. (2003). Phosphoinositide regulation of the actin cytoskeleton. *Annu. Rev. Physiol.* **65**, 761-789.
Zaidel-Bar, R., Ballestrem, C., Kam, Z. and Geiger, B. (2003). Early molecular events in the assembly of matrix adhesions at the leading edge of migrating cells. *J. Cell Sci.* **116**, 4605-4613.
Zamir, E., Katz, B. Z., Aota, S., Yamada, K. M., Geiger, B. and Kam, Z. (1999). Molecular diversity of cell-matrix adhesions. *J. Cell Sci.* **112**, 1655-1669.
Ziegler, W. H., Tigges, U., Zieseniss, A. and Jockusch, B. M. (2002). A lipid-regulated docking site on vinculin for protein kinase C. *J. Biol. Chem.* **277**, 7396-7404.